11th U.S. National Combustion Meeting
Organized by the Western States Section of the Combustion Institute
March 24–27, 2019
Pasadena, California

Boundary Layer Ignition Modeling

Stephanie A. Coronel[1,*], *Simon Lapointe*[1], *and Joseph E. Shepherd*[1]

[1]*Graduate Aerospace Laboratories, California Institute of Technology, Pasadena, CA*
[*]*Corresponding author:* stephaniecoronel@gmail.com

Abstract: A numerical study using detailed chemistry was performed on ignition within temporally evolving thermal boundary layers produced by a variation of the classical Rayleigh problem, impulsively accelerating and heating a wall. The study considers *n*-hexane-air boundary layers and gradients only in the wall normal direction. These calculations demonstrate how heat and momentum transfer compete with chemical reactions to create a reaction kernel within the boundary layer, some distance from the wall. Tracking a fluid parcel in *n*-hexane-air mixture reveals that just prior to ignition, significant variations in fuel composition may occur depending on the wall temperature. For a wall temperature of 1400 K, the parcel consists mostly of *n*-hexane; however, at a lower wall temperature of 1150 K, the parcel will have mostly decomposed into ethylene. Temperature and species histories of selected fluid parcel and space-time visualizations demonstrate how the ignition kernel is formed and a flame emerges out of the boundary layer into the surrounding flow.
Keywords: Ignition, Thermal Boundary Layer

1. Introduction

Hot surfaces can be created in the manufacturing, nuclear, and mining sectors by welding, cutting, grinding, and soldering processes. The motivation to study hot surface hazards stems from the possibility that an accidental explosion can occur within the thermal boundary layer of the surface that could possibly lead to damage to the surroundings, unsafe conditions, and most importantly, loss of life. Therefore, it is important to understand the underlying physics behind hot surface ignition which can be accomplished through numerical simulations of a thermal boundary layer. Several numerical studies have been performed on ignition adjacent to a heated surface. Kumar [1] performed a one-dimensional unsteady analysis of ignition of hydrogen-air adjacent to a vertical hot surface. The vertical motion of the gases due to buoyancy was neglected and only the motion normal to the heated surface was considered. The chemistry was modeled using multistep, chain-branching reactions of the modified Arrhenius type. Kumar [1] compared his calculations with experimental results of ignition by a vertical cylindrical igniter heated at 5 K/s and found them to be in excellent agreement for hydrogen-air mixtures even though the buoyancy induced flow was neglected. Chen and Faeth [2] performed simulations of flow adjacent to a vertical hot surface; the problem was treated as two-dimensional and steady, and the chemistry was modeled using a one-step reaction of the Arrhenius type. Chen and Faeth [2] assumed constant temperature as well as constant heat flux conditions on the heated wall. In addition, Chen and Faeth [2] determined that near the ignition threshold, a certain distance above the hot surface was needed for a deflagration wave to develop. Sano and Yamashita [3] performed thorough two-dimensional simulations of ignition in a methane-air laminar boundary layer over a horizontal hot plate.

The goal of this study is to gain insight into the processes leading to ignition in a *n*-hexane-air thermal boundary layer using a variation of the classical Rayleigh problem, impulsively heating a wall. Since a one-dimensional transient boundary layer is studied, rapid simulations are possible even with relatively detailed chemical reaction mechanisms.

2. Computational Methodology

Figure 1 illustrates the situation considered in the present study. The flow is transient but one-dimensional, all properties depend only on distance y and time t. All properties are independent of the wall-parallel distance x, i.e., $\partial/\partial x = 0$. At $t > 0$ the temperature at the wall is set to T_{wall}, where $T_{\text{wall}} > T_\infty$. Temporal growth of the thermal boundary layer is observed in Fig. 1, analogous to spatial growth over a flat hot surface. The problem illustrated in Fig. 1 was solved using the low Mach number Navier-Stokes equations.

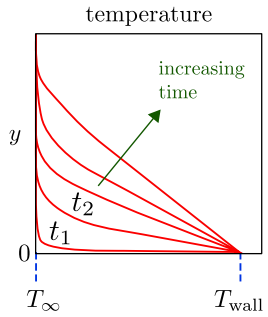

Figure 1: Temporal growth of thermal boundary layer by impulsively applied boundary conditions at $y = 0$ and $t > 0$; the gas temperature is T_∞ as $y \to \infty$, and T_{wall} at $y = 0$.

$$\frac{\partial \rho}{\partial t} + \nabla \cdot (\rho \mathbf{u}) = 0, \tag{1}$$

$$\frac{\partial (\rho \mathbf{u})}{\partial t} + \nabla \cdot (\rho \mathbf{u} \otimes \mathbf{u}) = -\nabla p + \nabla \cdot \tau, \tag{2}$$

$$\frac{\partial (\rho Y_i)}{\partial t} + \nabla \cdot (\rho \mathbf{u} Y_i) = -\nabla \cdot \mathbf{j}_i + \dot{\omega}_i \quad \text{where} \quad \mathbf{j}_i = -\rho D_i \frac{Y_i}{X_i} \nabla X_i - \rho Y_i \mathbf{u}_c, \tag{3}$$

$$\frac{\partial (\rho T)}{\partial t} + \nabla \cdot (\rho \mathbf{u} T) = \nabla \cdot (\rho \alpha \nabla T) - \frac{1}{c_p} \sum_k c_{p,i} \mathbf{j}_i \cdot \nabla T + \frac{\rho \alpha}{c_p} \nabla c_p \cdot \nabla T - \frac{1}{c_p} \sum_i h_i (T) \dot{\omega}_i + \frac{1}{c_p} \frac{\mathrm{D}p}{\mathrm{D}t} \tag{4}$$

In Eqs. 1 to 4, ρ is the fluid density, $\mathbf{u}$ is the velocity vector (u, v), p is the hydrodynamic pressure, τ is the viscous stress tensor, Y_i is the species mass fraction, T is the fluid temperature, ω_i is the species production rate, $\alpha = \lambda/(\rho/c_p)$ is the mixture thermal diffusivity, c_p is the mixture specific heat capacity, $c_{p,i}$ is the species specific heat capacity, h_i is the species enthalpy at T, $\mathbf{j}_i$ is the diffusive mass-flux vector, D_i is the mixture averaged diffusion coefficient for species i, X_i

is the species mole fraction, and $\mathbf{u}_c = -\sum_i D_i \frac{Y_i}{X_i} \nabla X_i$ is a correction velocity that enforces zero net mass diffusion flux. Eqs. 1 to 4 are completed with the equation of state: $P_o = \rho \tilde{R} T \sum Y_i / W_i$, where P_o is the thermodynamic pressure, W_i is the species molecular weight, and $\tilde{R}$ is the universal gas constant. The species thermal conductivities λ_i were computed using Eucken's formula [4], and the mixture-averaged thermal conductivity, λ, was obtained from the empirical formula described in Mathur et al. [5]. The species viscosities, μ_i, were calculated using standard gas kinetic theory [6] and the mixture-averaged viscosity, μ, was calculated using Wilke's mixture rule [7]. The individual species molecular diffusivities, D_i, were calculated as $D_i = \alpha / Le_i$, where Le_i is the species Lewis numbers. In the present study, the Lewis numbers were treated as constant but non-unity. The governing equations were solved using the structured, multi-physics and multi-scale finite difference code NGA [8]. The time integration was performed using a second-order semi-implicit Crank-Nicolson scheme. Lagragian particle tracking was implemented to track the history of fluid parcels. The present study used an *n*-hexane-air mechanism (62 species, 226 reactions) reduced from the mechanism described in Mével et al. [9] using the methods of Davidenko et al. [10].

Since $\partial / \partial x = 0$, the x-direction momentum equation was decoupled from the other governing equations; therefore, the value of the freestream velocity did not influence the solutions except for u itself. The evolution of the thermal boundary layer was initiated by impulsively applying the following boundary conditions:

$$y = 0 \quad \text{and} \quad t > 0: \quad v = 0, T = T_{\text{wall}}, \frac{\partial Y_i}{\partial y} = 0 \tag{5}$$

$$y \to \infty \quad \text{and} \quad t > 0: \quad \frac{\partial v}{\partial y} = 0, T = T_\infty, Y_i = Y_{i,\infty}. \tag{6}$$

The initial conditions were:

$$v = 0, T = T_\infty, Y_i = Y_{i,\infty} \quad \text{for} \quad 0 \leq y < \infty. \tag{7}$$

3. *n*-Hexane-Air Results

Simulations were performed with *n*-hexane-air at $\Phi = 0.9$ and an initial temperature and pressure of 300 K and 100 kPa, respectively. Figure 2 (a) $T_{\text{wall}} = 1150$ K and (b) $T_{\text{wall}} = 1400$ K shows filled contours of temperature and a contour line at 303 K to illustrate the evolution of the thermal boundary layer, the ignition, and the subsequent flame propagation. A flame originates deep within the boundary layer and propagates outward into the cold surrounding gas. The flame is indicated by the thin layer of sudden temperature increase. Ignition occurs at approximately 101 ms for $T_{\text{wall}} = 1150$ K at 2 ms for $T_{\text{wall}} = 1400$ K. Ignition is quantified as the time at which the gas temperature exceeds 150 K over the wall temperature.

3.1 Fluid Parcel: Temperature and Species Mass Fractions

Figures 3 show the evolution of species products and reactants, and intermediates along selected fluid parcel paths ($y_0 = 150$ μm) for the two wall temperature cases shown in Fig. 2. Figure 3 (a) shows a linear depletion (log scale) of the fuel to 2.31×10^{-3} at 100 ms. Prior to rapid consumption

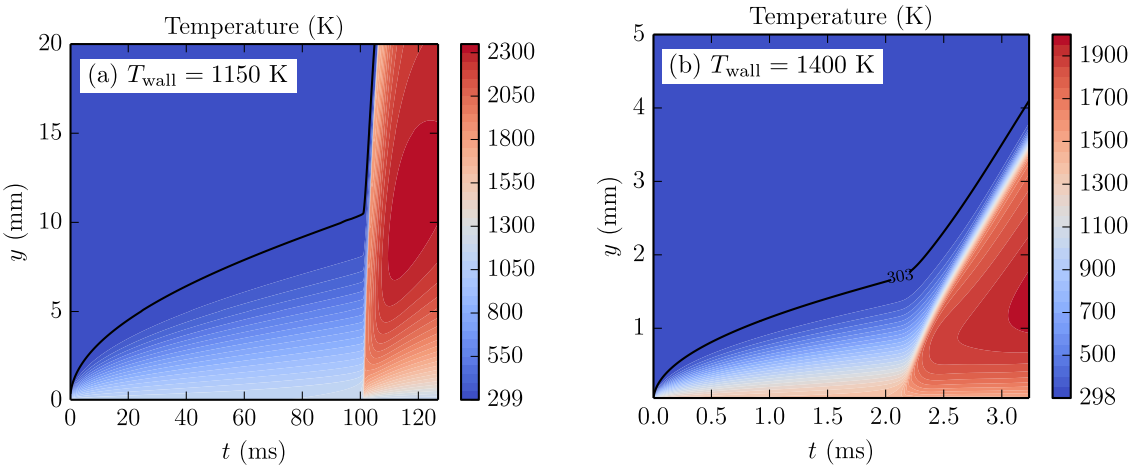

Figure 2: Temporal and spatial evolution of the thermal boundary layer and the subsequent ignition and flame propagation for (a) $T_{\text{wall}} = 1150$ K and (b) $T_{\text{wall}} = 1400$ K.

of the fuel, there is minimal decrease in O_2 indicating that fuel depletion is due to decomposition of *n*-hexane into smaller fuel molecules. A similar trend in the fuel and oxidizer is observed for the higher wall temperature case shown in Fig. 3 (b); however, the depletion of the fuel prior to rapid consumption stops at 2.0 ms; at 2.0 ms, the fuel mass fraction is 2.47×10^{-2}, an order of magnitude larger than the low temperature case fuel mass fraction prior to ignition. The unimolecular decomposition of the three isomeric forms of the $\dot{\mu}$ radical (C_6H_{13}) which are produced by H abstraction, lead to the creation of several fuels: ethylene (C_2H_4), methane (CH_4), propene (C_3H_6), ethane (C_2H_6), 1-butene (C_4H_8-1), and 1-pentene (C_5H_{10}-1), as well as small amounts of H_2 [11]. In Fig. 3 (a), a significant amount of C_2H_4 is produced at 30 ms until it peaks at approximately 65 ms. The mass fraction of C_2H_4 is higher than that of *n*-hexane at ignition. A similar pattern is observed in Fig. 3 (b); however, smaller amounts of the secondary fuel mass fraction are created since the decomposition of *n*-hexane along the fluid parcel trajectory is not as extensive.

3.2 Temperature and Species Mass Fractions Profiles: $T_{\text{wall}} = 1150$ K

Figure 4 shows the temperature profiles at different times leading up to ignition for a wall temperature of 1150 K. Figure 4 (a) shows thermal energy diffusing away from the hot wall; after 100 ms, the thermal boundary layer grows to a thickness of approximately 10 mm. At 100.1 ms there is a temperature increase a distance of 0.55 mm away from the wall, this location is where the ignition event originates according to the 150 K ΔT ignition criterion. Over the next 2 ms, the flame propagates away from this location as indicated by the rapid development of the gas temperature shown in 4 (b). Initially, the maximum temperature reached is 1700 K at 101.3 ms; however, it continues to increase to 1900 K at 101.7 ms. The maximum temperature increases rapidly in time as the flame moves away from the wall propagating into increasing concentrations of the fuel mass fraction, shown in Fig. 5 (b). The flame front is marked by the large temperature gradient observed at 2, 3, 4 ,and 5.5 mm at 101.3, 101.5, 101.7. and 101.2 ms, respectively. Figure 5 (a) shows the depletion of *n*-hexane as it is decomposed into smaller fuel molecules. At a given time, the fuel mass

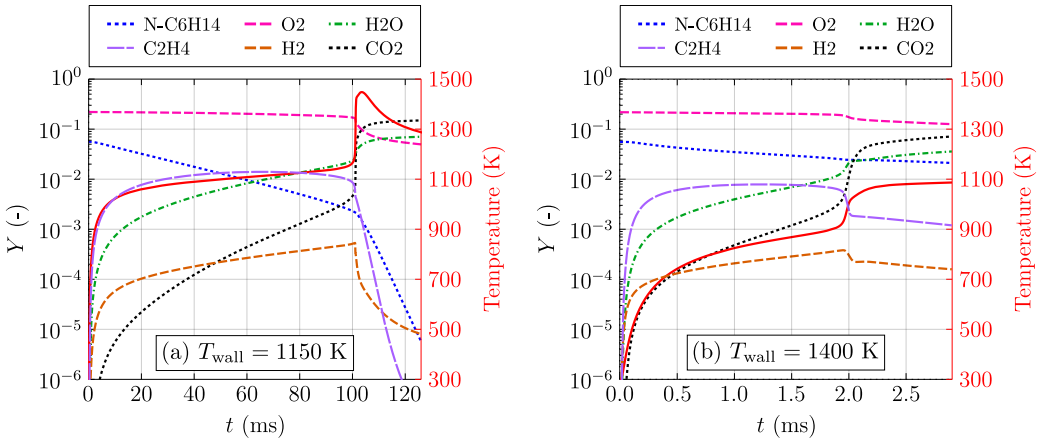

Figure 3: Species mass fractions (left-axis) and temperature (right-axis and solid line) along fluid parcel path ($y_0 = 150$ μm) for (a) $T_{wall} = 1150$ K and (b) $T_{wall} = 1400$ K.

fraction decreases as y approaches 0, i.e., as the gas temperature increases from the freestream to the wall temperature. At 100.1 ms, the depletion of n-hexane extends up to 7 mm away from the wall and is fully depleted at at $y = 0-1$ mm. Although a temperature increase is already observed at 100.1 ms (see Fig. 4 (a)), rapid consumption of the fuel does not start until 101.3 ms, shown in Fig. 5 (b). This indicates that the formation of a self-sustained flame occurs approximately 1 ms after the initial heat release. Figure 6 (a) shows that the formation of C_2H_4 occurs across the thermal boundary layer with the lowest concentration near the thermal boundary layer edge. At the wall, the C_2H_4 mass fraction exceeds 1.5% at 55.6 ms; at this time and location, n-hexane has been depleted to less than 0.5%. C_2H_4 is depleted at $t > 55.6$ ms and rapid consumption starts at 101.3 ms, shown in Fig. 6 (b).

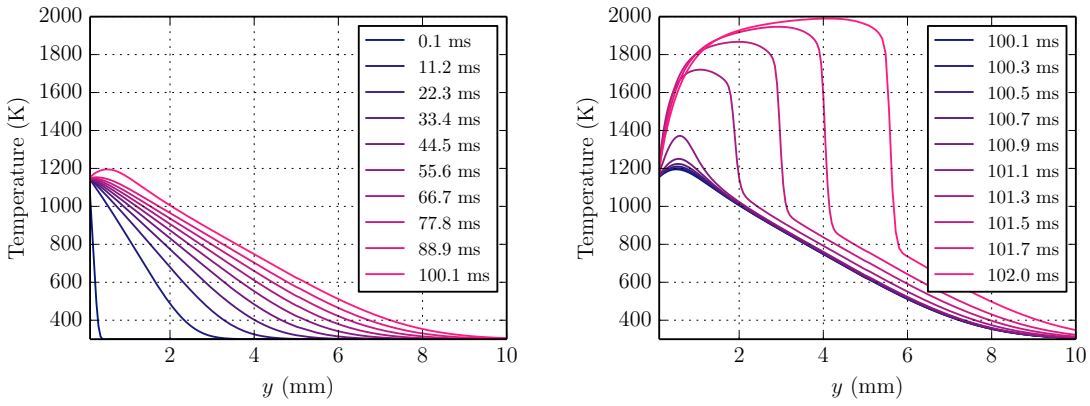

Figure 4: Spatial profiles of temperature within the thermal boundary layer for $T_{wall} = 1150$ K at (a) $t = 0.1-100.1$ ms and (b) $t = 100.1-102.0$ ms.

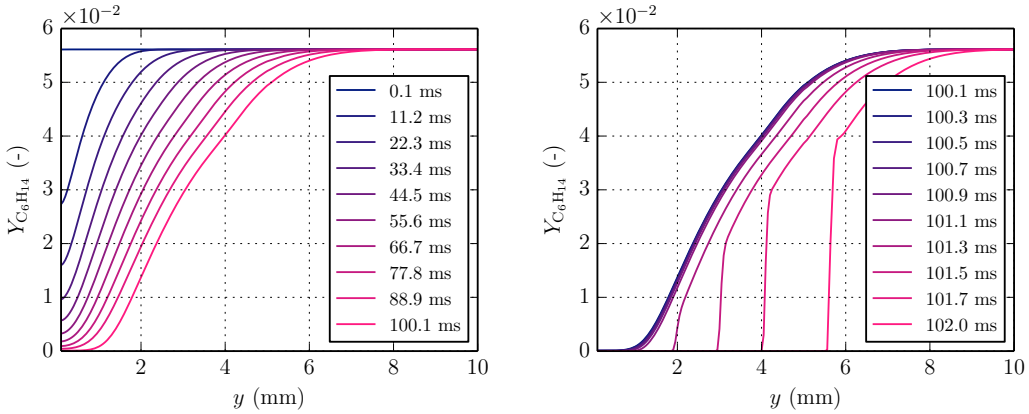

Figure 5: Spatial profiles of *n*-hexane mass fraction within the thermal boundary layer for $T_{\text{wall}} = 1150$ K at (a) $t = 0.1 - 100.1$ ms and (b) $t = 100.1 - 102.0$ ms.

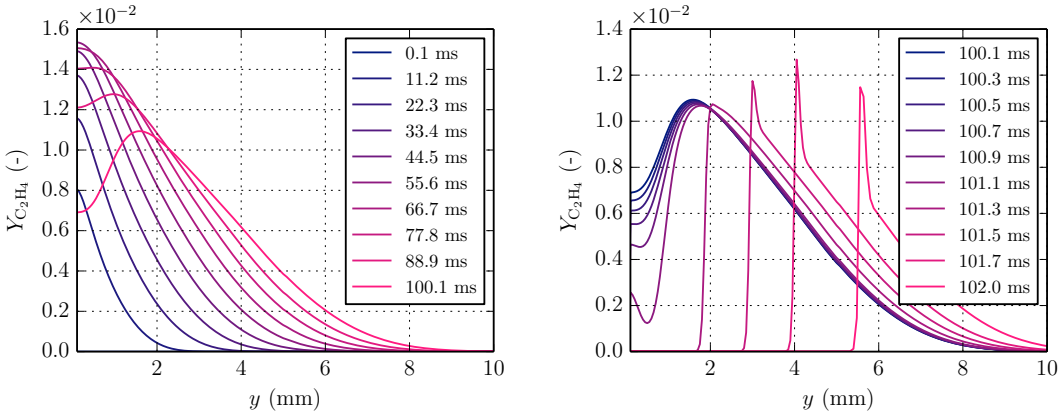

Figure 6: Spatial profiles of C_2H_4 mass fraction within the thermal boundary layer for $T_{\text{wall}} = 1150$ K at (a) $t = 0.1 - 100.1$ ms and (b) $t = 100.1 - 102.0$ ms.

3.3 Temperature and Species Mass Fractions Profiles: $T_{\text{wall}} = 1400$ K

An increase in temperature, above the wall temperature of 1400 K, is first observed at 2.101 ms. The rise in temperature first occurs at approximately 0.06 mm away from the wall marking the onset of the ignition event. The flame appears at 2.332 ms, shown in Fig. 7 (b) by the large temperature gradient. Figure 8 (a) shows that the decomposition of *n*-hexane occurs across the thermal boundary layer; the decrease in the fuel mass fraction is observed up to 1.25 mm (72% of thermal boundary layer (TBL) thickness) at 2.101 ms. Due to the higher gas temperature, compared to the $T_{\text{wall}} = 1150$ K case, the decomposition of *n*-hexane occurs rapidly, falling to 0.5% over 0.234 ms. Comparable decay occurs over 44.5 ms for $T_{\text{wall}} = 1150$ K. When the first increase in gas temperature above 1400 K is observed for $T_{\text{wall}} = 1400$ K, the *n*-hexane mass fraction has dropped to zero at $y = 0 - 0.25$ mm. Figure 9 (a) shows the rapid creation of C_2H_4 (1.9%) at the wall at 0.001 ms. Later, at 0.7011 ms, the C_2H_4 begins to be depleted at the wall and

to a lesser extent away from it. Figure 9 (b) shows the C_2H_4 distribution becoming narrower in time, indicating the formation of a flame.

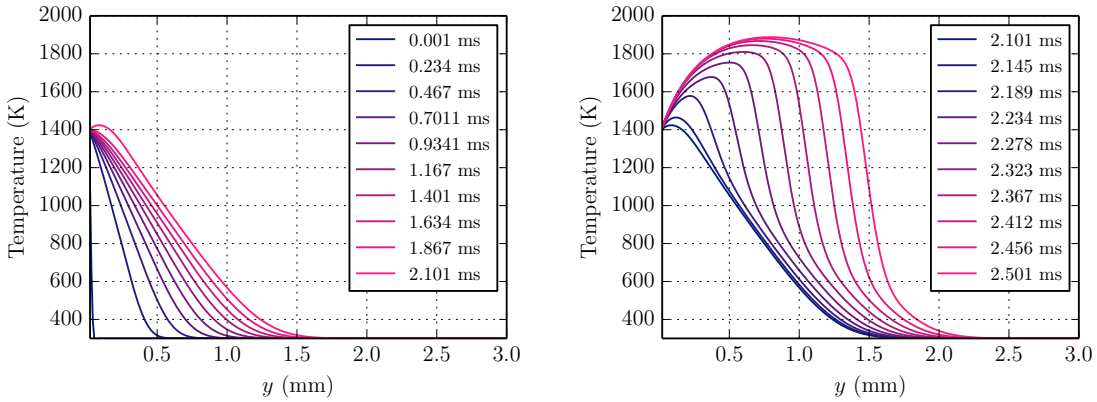

Figure 7: Spatial profiles of temperature within the thermal boundary layer for $T_{\text{wall}} = 1400$ K at (a) $t = 0.001 - 2.101$ ms and (b) $t = 2.101 - 2.501$ ms.

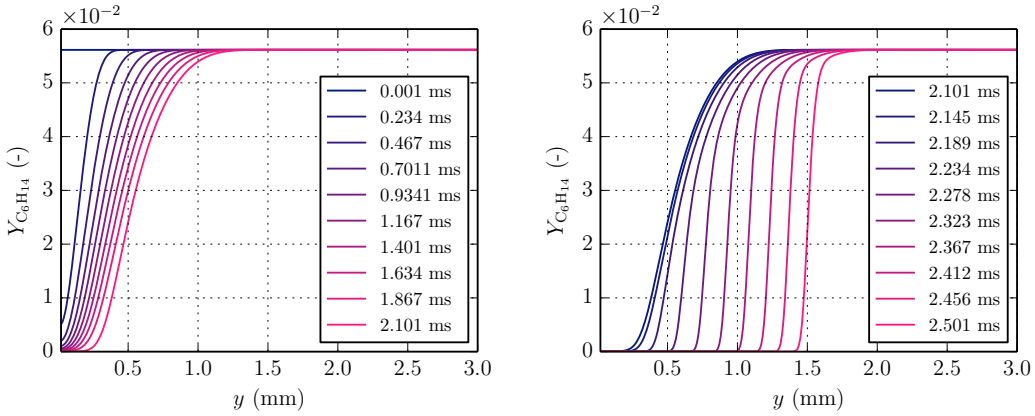

Figure 8: Spatial profiles of C_6H_{14} mass fraction within the thermal boundary layer for $T_{\text{wall}} = 1400$ K at (a) $t = 0.001 - 2.101$ ms and (b) $t = 2.101 - 2.501$ ms.

3.4 Ignition Criterion

Figure 10 shows the temperature history of several fluid parcels for $T_{\text{wall}} = 1400$ K; the legend corresponds to the originating location, y_0, of each fluid parcel. The fluid parcels closest to the wall are rapidly heated, e.g., the fluid parcel next to the wall, $y_0 = 0.004$ mm, reaches 99% of the wall temperature within 0.05 ms. Although that is the fluid parcel with the highest temperature, it does not ignite since any thermal energy released through chemical reactions is lost by conduction to the wall. The figure inset shows temperature histories for selected fluid parcels. A continuous range of temperature increase is observed with increasing distance from the wall. Based on the temperature history, the first igniting fluid parcel cannot be distinguished. Earlier, ignition was defined by the

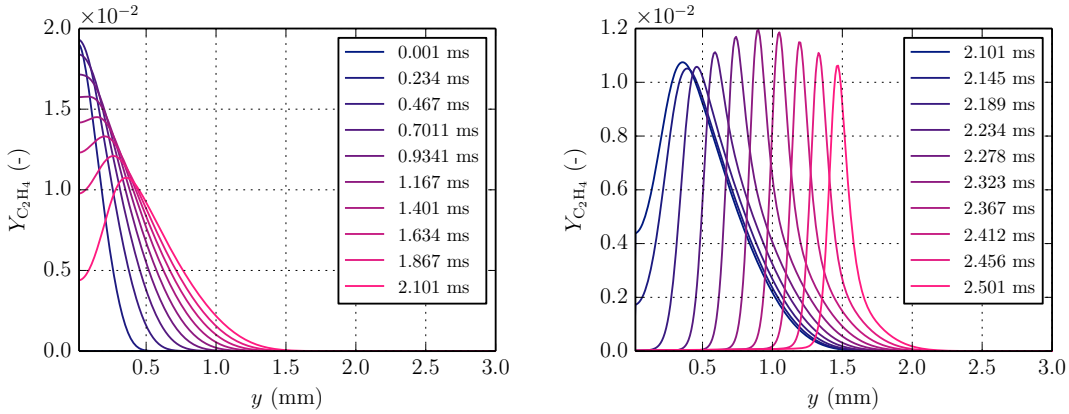

Figure 9: Spatial profiles of C_2H_4 mass fraction within the thermal boundary layer for $T_{\text{wall}} = 1400$ K at (a) $t = 0.001 - 2.101$ ms and (b) $t = 2.101 - 2.501$ ms.

time and location when a temperature increase of $\Delta T = 150$ K over the wall temperature (reference temperature) was first observed. In the figure inset, this ΔT criterion corresponds to igniting fluid parcels originating at $y_0 = 0.05$ and 0.054 mm; however, the choice of defining a ΔT to mark ignition is rather arbitrary. Using a reference temperature equivalent to the wall temperature is suitable if the entire domain is initially at this temperature, but this is not the case in thermal boundary layer flows adjacent to a hot wall. In the thermal boundary layer, the gas has a range of temperatures, e.g., the figure inset shows fluid parcel temperatures ranging from 1200 K to over 1350 K at 1.8 ms. A different criterion is needed to pinpoint the ignition location and time that does not rely on picking an arbitrary value such as ΔT. One option is to look at the evolution of a specific species mass fraction along the fluid parcel paths. Figure 11 shows the CO species mass fraction along several fluid parcel trajectories; the fluid parcels that have the highest peak in CO correspond to $y_0 = 0.05$ and 0.054 mm. The second highest peak is given by $y_0 = 0.235$ mm; however, this particular fluid parcel is encountering a propagating flame well after the ignition event. An ignition criterion based on the maximum concentration in CO is still somewhat arbitrary since other species can be used that would yield slightly different results; however, a peak is a well defined feature when compared to an arbitrary value of ΔT. Using the peak in CO mass fraction as the ignition criterion, the ignition location corresponds to the $y_0 = 0.058$ mm fluid parcel. At the ignition time of 2.23 ms, the fluid parcel is approximately 0.26 mm away from the wall (15% of the TBL thickness).

4. Conclusions

A numerical study was performed on ignition within a temporally evolving thermal boundary layer of *n*-hexane-air using detailed chemistry. The temperature history of a fluid parcel had an significant effect on the gas composition prior to ignition. The long delay times corresponding to a wall temperature of 1150 K resulted in *n*-hexane decomposing into smaller fuel molecules before ignition. Just prior to ignition, the main fuel species present was ethylene. At a higher wall temperature of 1400 K, the *n*-hexane did not undergo significant decomposition and prior to ignition the main

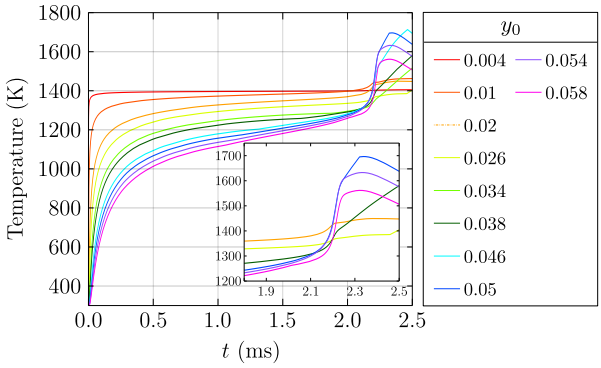

Figure 10: Temporal evolution of temperature of fluid parcels for $T_{\text{wall}} = 1400$ K case; the units of the initial fluid parcel location, y_0, are given in mm.

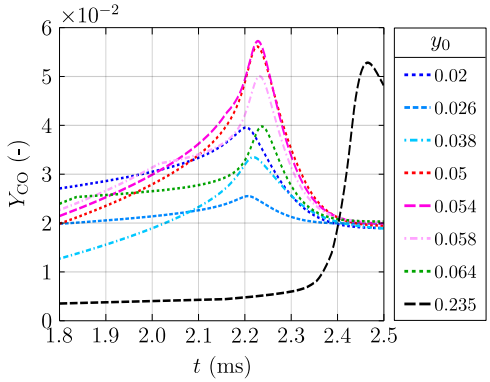

Figure 11: Temporal evolution of CO mass fraction of select fluid parcels; the units of the initial fluid parcel location, y_0, are given in mm.

fuel species was still *n*-hexane. It was also evident from spatial plots of the fuel and temperature, that ignition always occurred some distance away from the wall. The fuel profiles indicated that prior to any temperature increase resulting from chemical reactions, a thin region normal to the wall had already been decomposed to produce secondary fuels. The width of this depleted region was 1 mm for $T_{\text{wall}} = 1150$ and 0.25 mm for $T_{\text{wall}} = 1400$ K, corresponding to $7 - 10\%$ of their respective thermal boundary layer thicknesses. The use of fluid parcel tracking allowed us to analyze the behavior of several fluid parcels close to the hot wall. The temperature and species mass fraction of CO allowed us to pinpoint the igniting fluid parcel based on the ignition criterion that uses the peak in CO to mark ignition.

5. Acknowledgements

This work was carried out in the Explosion Dynamics Laboratory of the California Institute of Technology, and was supported by The Boeing Company through a Strategic Research and Development Relationship Agreement CT-BA-GTA-1.

References

[1] R. Kumar, Ignition of hydrogen-oxygen-diluent mixtures adjacent to a hot, nonreactive surface, Combustion and Flame 75 (1989) 197–215.

[2] L.-D. Chen and G. Faeth, Ignition of a combustible gas near heated vertical surfaces, Combustion and Flame 42 (1981) 77–92.

[3] T. Sano and A. Yamashita, Flame Ignition of Premixed Methane Air Mixtures on a High-Temperature Plate, JSME International Journal Series B 37 (1994) 180–186.

[4] A. Eucken, The heat-carrying capabilities, the specific heat and the internal friction of gas, Physikalische Zeitschrift 14 (1913) 324–332.

[5] S. Mathur, P. K. Tondon, and S. C. Saxena, Thermal conductivity of binary ternary and quaternary mixtures of rare gases, Molecular Physics 12 (1967) 569–579.

[6] J. Hirschfelder, C. Curtiss, and R. Bird, Molecular theory of gases and liquids, Wiley, 1954.

[7] C. R. Wilke, A Viscosity Equation for Gas Mixtures, The Journal of Chemical Physics 18 (1950) 517–519.

[8] O. Desjardins, G. Blanquart, G. Balarac, and H. Pitsch, High order conservative finite difference scheme for variable density low Mach number turbulent flows, Journal of Computational Physics 227 (2008) 7125–7159.

[9] R. Mével, K. Chatelain, P. A. Boettcher, and J. E. Shepherd, Low temperature oxidation of *n*-hexane in a flow reactor, Fuel 126 (2014) 282–293.

[10] D. Davidenko, R. Mével, and G. Dupré, Reduced kinetic scheme for the simulation of detonation in H_2-N_2O-Ar mixtures, Proceedings of the European Combustion Meeting 4 (2009) 6.

[11] P. Malacarne, F. Billaud, and F. Baronnet, Thermal decomposition of 3-methylpentane and *n*-hexane: Reaction mechanism and correlations between structure and formation of light olefins, Journal of Analytical and Applied Pyrolysis 12 (1987) 243–256.